Optics Letters

Plasmonic *Zitterbewegung* in binary graphene sheet arrays

YANG FAN,[1,2] BING WANG,[1,*] HE HUANG,[1] KAI WANG,[1] HUA LONG,[1] AND PEIXIANG LU[1,3]

[1]Wuhan National Laboratory for Optoelectronics and School of Physics, Huazhong University of Science and Technology, Wuhan 430074, China
[2]College of Science, Naval University of Engineering, Wuhan 430033, China
[3]e-mail: lupeixiang@hust.edu.cn
*Corresponding author: wangbing@hust.edu.cn

Received 12 January 2015; revised 24 May 2015; accepted 24 May 2015; posted 26 May 2015 (Doc. ID 232256); published 16 June 2015

We theoretically investigate the plasmonic *Zitterbewegung* (ZB) effect in binary graphene sheet arrays (GSAs). The surface plasmon polariton (SPP) modes of two minibands are realized by alternately varying the chemical potentials of individual graphene sheets in the arrays. Numerical simulations show that SPPs in the array experience characteristic trembling motion. The oscillating periods of the plasmonic ZB are strongly dependent on the propagation constant mismatch and varied in the range of micrometer, while the amplitude reaches tens of nanometers, making the ZB effect easier to be observed in practice.

OCIS codes: (240.6680) Surface plasmons; (230.7370) Waveguides; (160.3918) Metamaterials.

http://dx.doi.org/10.1364/OL.40.002945

The relativistic electrons may exhibit a rapid trembling motion around their average trajectory in the absence of external fields, which is known as *Zitterbewegung* (ZB), introduced by Schrödinger in 1930. The ZB arises from the interference between the positive and negative energy bands, and the characteristic period of the motion is determined by the bandgap. It is hard to directly observe the ZB effect experimentally because of the small amplitude and the large oscillation frequency. Many theoretical studies have been reported in analogizing this phenomenon in semiconductors [1], trapped ions [2], photonic crystals [3], metamaterials [4], and dielectric waveguide arrays [5]. The ZB effect has also been demonstrated numerically in binary metallic waveguide arrays [6].

Recently, the graphene-supported surface plasmon polaritons (SPPs) have drawn much attention due to their promising applications. Graphene exhibits a stronger SPP field confinement and lower propagation loss compared with metals [7]. Moreover, the surface conductivity of graphene can be flexibly tuned by chemical doping or external static electric and magnetic fields. These features make graphene a competitive alternative to metals in manipulating SPPs [8,9]. Various interesting optical phenomena are observed in graphene structures, such as hyperlense [10], negative refraction [11], and discrete Talbot effect [12].

In this Letter, we shall study the plasmonic ZB phenomenon in binary graphene sheet arrays (GSAs). It should be mentioned that the ZB of SPPs is substantially different from that of electrons in graphene. The latter has been intensively investigated previously [13–15], which refers to the temporal trembling motion of electrons with a very short period of several femtoseconds. The SPPs in ZB motion are governed by the similar Dirac equation of electrons, but for trembling in real space. In order to observe plasmonic ZB, two SPP bands are needed to mimic the positive-energy band and negative-energy band of a relativistic electron. Thus we build up the binary GSAs by alternative spatial arrangement of graphene waveguides with two different chemical potentials. Numerical simulations are performed to verify the ZB for SPPs in this structures.

The schematic diagram of the binary GSAs is shown in Fig. 1(a). The graphene sheets are embedded in the dielectric medium with a relative permittivity denoted by ϵ_d. The interlayer space of graphene in the array is labeled with d. The surface conductivity of graphene σ is modeled by using the Kubo formula, which depends on the graphene chemical potential μ_c, electron relaxation time τ, and temperature T [16]. We alternately vary two different graphene sheets A and B with

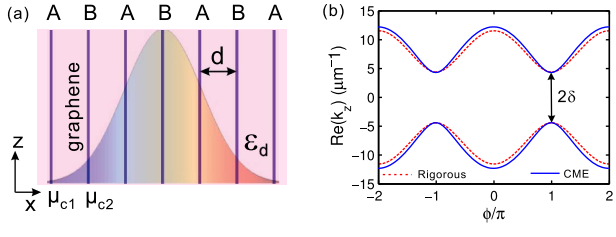

Fig. 1. (a) Schematic of binary GSAs, made of two interleaved graphene waveguides A and B with chemical potential μ_{c1} and μ_{c2} changes, equally spaced by d. The period of the binary GSAs is $2d$. Inset plots spatial phase of the incident beam with a Gaussian envelope. (b) Diffraction relations of the binary GSAs comprising two bands separated by 2δ. The dashed and solid curves are the results calculated by the rigorous method [Eq. (1)] and coupled-mode equation [Eq. (2)], respectively.

chemical potential μ_{c1} and μ_{c2} ($\mu_{c2} > \mu_{c1}$) in the guide array to achieve two SPP bands. The relaxation time τ of electrons in graphene is given by $\tau = \mu\mu_c/(ev_F^2)$, where e is the electron charge, and $v_F = 10^6$ m/s is the Fermi velocity. The DC mobility μ of electrons in high-quality suspended graphene can reach over 100,000 $cm^2\ V^{-1}\ s^{-1}$ at room temperature $T = 300$ K [17]. In our study, the incident wavelength $\lambda = 10$ μm and the interlayer space $d = 30$ nm is initially considered.

The dispersion relation of collective SPP mode in binary GSAs is given by using the transfer matrix method and imposing the Bloch theorem [18]

$$\cos^2\left(\frac{\phi}{2}\right) = \left[\cosh(\kappa d) - \frac{\kappa\xi_1}{2}\sinh(\kappa d)\right]\left[\cosh(\kappa d) - \frac{\kappa\xi_2}{2}\sinh(\kappa d)\right], \tag{1}$$

where $\kappa = \sqrt{k_z^2 - \epsilon_d k_0^2}$, with k_z the wave vector of SPPs in the z direction and $k_0 = 2\pi/\lambda$ the wave vector in air. The Bloch momentum in the x direction is denoted by $\phi = k_x(2d)$ and $\xi_i = \frac{\eta_0\sigma_i}{i\epsilon_d k_0}$ being the plasmonic thickness in the single-layer graphene sheet A or B [19].

By considering only nearest-neighbor couplings, the normalized amplitude of field distributions in one-dimensional waveguide arrays obey the linear coupled-mode equation (CME) [20,21]

$$i\frac{da_n}{dz} = C_g(a_{n-1} + a_{n+1}) + (-1)^n\delta a_n, \tag{2}$$

where a_n represents the modal amplitude in the nth graphene sheet site, and C_g and 2δ are the coupling coefficient and the propagation constant mismatch between two adjacent graphene sheets. The dispersion relation of the structure can be obtained from Eq. (2) by assigning to a_n the form $a_n = \exp[in(2k_x d)]\exp(ik_z z)$ and reads [21]

$$k_z = \pm[\delta^2 + 4C_g^2\cos^2(k_x d)]^{1/2}. \tag{3}$$

The diffraction curves of the super SPP modes in the binary GSAs for $\mu_{c1} = 0.15$ eV and $\mu_{c2} = 0.18$ eV are plotted in Fig. 1(b). The binary GSAs support two symmetric minibands separated by a gap of width 2δ at boundaries of the Brillouin zone ($k_x = \frac{\pi}{2d}$). The diffraction curves are similar to the typical hyperbolic energy-momentum dispersion relations of a freely moving relativistic massive particle, which suggests that SPP beam propagation in the binary GSAs for Bloch waves with wave number k_x close to $\frac{\pi}{2d}$ mimics the dynamics of the relativistic Dirac equation. The curves obtained from Eq. (3) (solid curves) agree with rigorous computations (dashed curves) verifying that the coupled-mode model holds well in the binary GSAs structure. To excite plasmonic ZB in the binary GSAs effectively, adjacent waveguides are excited with a phase difference of $\pi/2$, as shown in the inset of Fig. 1(a). After setting $a_n(z) = (-1)^n\psi_1(n,z)$ and $a_{n+1}(z) = -i(-1)^n\psi_2(n,z)$ in Eq. (2) and introducing the continuous spatial coordinate $n \to x$, we arrive at a two-component wave function $\psi = (\psi_1, \psi_2)^T$ formally satisfies the one-dimensional Dirac equation [5,6]

$$i\frac{\partial\psi}{\partial z} + iC_g\alpha\frac{\partial\psi}{\partial x} - \delta\beta\psi = 0, \tag{4}$$

where $\alpha = \begin{pmatrix} 0 & 1 \\ 1 & 0 \end{pmatrix}$ and $\beta = \begin{pmatrix} 1 & 0 \\ 0 & -1 \end{pmatrix}$ are the Pauli matrices. Therefore, the central position of SPP beam $x_c(z) = \Sigma x(|a_n|^2 + |a_{n+1}|^2)/\Sigma(|a_n|^2 + |a_{n+1}|^2)$ is expected to rapidly oscillate around its average trajectory, resulting in the ZB effect [21]. According to Eq. (4), the trajectory of the central position of SPP beam can be approximated as

$$x_c(z) = x_c(0) + v_0 z - \left(\frac{C_g}{2\delta}\right)\sin(2\delta z), \tag{5}$$

where v_0 is the mean shift speed of the SPP beam center and is proportional to C_g^3/δ^2 [22]. The last term representing of SPP oscillation in Eq. (5) suggests the ZB effect. The amplitude R_Z and period P_Z of the plasmonic ZB can be written as

$$R_Z = \frac{|C_g|d}{2\delta}, \qquad P_Z = \pi/\delta. \tag{6}$$

In order to calculate the ZB amplitude and period, we calculated the coupling coefficient C_g and propagation constant mismatch 2δ between the two different guides of binary GSAs through a method similar to that used in [23]. The C_g value of SPPs between adjacent guides of the GSAs is $C_g = (C_{g1} + C_{g2})/2$, where the values of C_{g1} and C_{g2} are the coupling coefficients in the homogeneous GSAs with the chemical potential μ_{c1} and μ_{c2}, which can be derived as $C_g = (\beta_e - \beta_o)/4$, with β_e and β_o being the propagation constants of the even and odd collective modes of the GSAs system, respectively [12]. Note that the even collective mode has a smaller propagation constant than the odd mode. As a result, the coupling coefficient is negative, which will result in a negative transverse shift of SPPs in the binary GSAs. The propagation constant mismatch is $2\delta = \beta_1 - \beta_2$, where the values of β_1 and β_2 are the propagation coefficients in the homogeneous GSAs with the chemical potential μ_{c1} and μ_{c2}, which is given by $\beta = (\beta_e + \beta_o)/2$ [24]. Figure 2 shows the values of C_g (red line) and 2δ (blue line) of SPPs in the binary GSAs by varying the chemical potential difference $\Delta\mu_c$ between graphene sheets A and B while $\mu_{c1} = 0.15$ eV, and the interlayer space is fixed at $d = 30$ nm. From Fig. 2, we see that the absolute values of C_g in the binary GSAs are decreased with increasing chemical potential difference $\Delta\mu_c$, while the values of propagation constant mismatch are increased with increasing $\Delta\mu_c$. According to Eq. (6), the calculated amplitudes and periods of plasmonic ZB

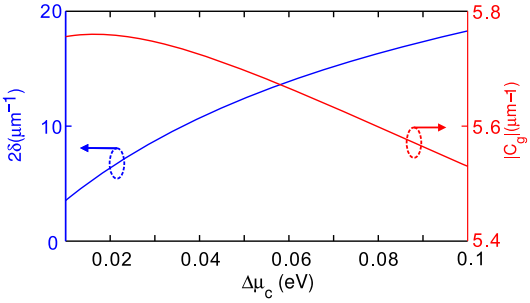

Fig. 2. Propagation constant mismatch 2δ (blue line) and coupling coefficient C_g (red line) between the two adjacent guides versus the chemical potential difference $\Delta\mu_c$ when $\mu_{c1} = 0.15$ eV is fixed.

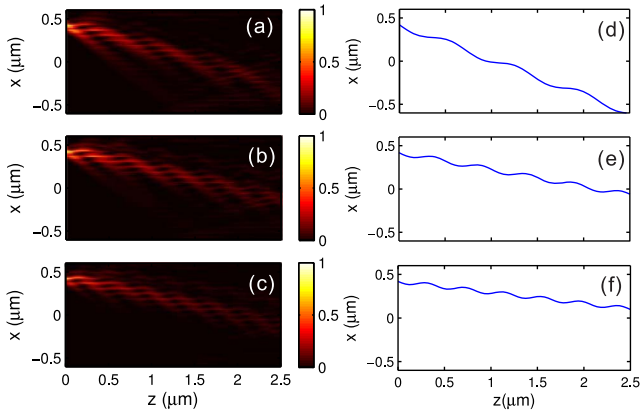

Fig. 3. Evolution of beam intensity ($|E|^2$) in the binary GSAs (a)–(c) and corresponding central positions x_c of SPP beams (d)–(f) as the chemical potential difference $\Delta\mu_c$ = [(a), (d)] 0.03 eV, [(b), (e)] 0.05 eV, and [(c), (f)] 0.07 eV, respectively.

are $R_Z = 20$, 14, and 11 nm and $P_Z = 720$, 506, and 414 nm as $\Delta\mu_c = 0.03$, 0.05, and 0.07 eV, respectively.

The steady electromagnetic field distributions are numerically calculated to verify the above analytical results. The computations are performed by using the FDFD method [25,26], where the graphene sheets are assumed to be freestanding in air with $\epsilon_d = 1$. Graphene is equivalent to a very thin metal film with a thickness of $\Delta = 1$ nm. Thus we can define an equivalent bulk permittivity for graphene given by $\epsilon_g = 1 + i\sigma_g\eta_0/(k_0\Delta)$ while $\eta_0 \approx 377\Omega$ represents the air impedance. The minimum mesh size equals 0.2 nm in the FDFD calculation. To excite plasmonic ZB in the binary GSAs effectively, a TM-polarized Gaussian beam is incident into the binary GSAs with the phase difference of $\pi/2$ between adjacent waveguides. The distributions of simulated electric field intensity ($|E|^2$) of SPP beams at different $\Delta\mu_c$ are shown in Figs. 3(a)–3(c), and the corresponding beam center positions x_c are shown in Figs. 3(d)–3(f). The trembling motions of the SPP beam are observed clearly, which correspond to the plasmonic ZB effect. Both the period and the amplitude of the oscillation decrease as $\Delta\mu_c$ increases. The simulated amplitudes and periods of plasmonic ZB are $R_Z = 20$, 16, and 12 nm and $P_Z = 750$, 500, and 400 nm as $\Delta\mu_c = 0.03$, 0.05, and 0.07 eV, respectively, which qualitatively agree with the analytic results acquired by Eq. (6). The centers of SPP beams undergo the negative transverse shifts, and the shift is reduced as $\Delta\mu_c$ increases, which is due to the fact that the shift speed v_0 decreases as $\Delta\mu_c$ increases according to Eq. (5).

The relations of ZB amplitude R_Z and period P_Z versus the chemical potential difference $\Delta\mu_c$ between graphene sheets A and B are explored. The values of R_Z and P_Z under different $\Delta\mu_c$ are plotted in Fig. 4. One can see that R_Z and P_Z decrease as $\Delta\mu_c$ increases. These numerical results of R_Z and P_Z are consistent with our general predictions acquired by using Eq. (6).

Finally, the ZB period P_Z as a function of the interlayer space (d) and wavelength (λ) while $\mu_{c1} = 0.15$ eV and $\mu_{c2} = 0.18$ eV is depicted in Fig. 5 for embedding materials of air ($\epsilon_d = 1$) and KCl ($\epsilon_d = 2.13$). The period of ZB depends weakly on d due to hyperbolic dispersion around the boundaries of the Brillouin zone. When the incident wavelength

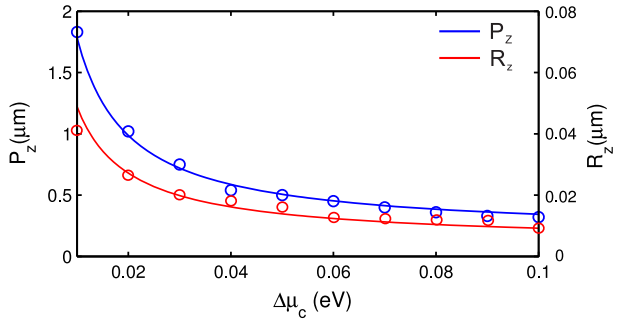

Fig. 4. Dependence of the ZB amplitude R_Z (red line) and period P_Z (blue line) on the chemical potential difference $\Delta\mu_c$ between graphene sheets A and B. The lines and markers represent the analytical and numerical results, respectively.

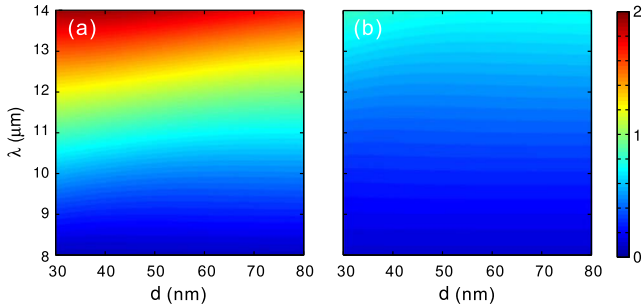

Fig. 5. Influence of the interlayer space, wavelength on P_Z for different embedding materials: (a) air and (b) KCl.

varies, we can also observe plasmonic ZB occurring in the same binary GSAs. P_Z increases with the incident wavelength λ increases. Furthermore, the value of P_Z decreases as the permittivity of embedding material increases.

In conclusion, we have demonstrated that plasmonic ZB can be excited in a wide range of wavelengths in binary GSAs. SPP modes of the two bands are realized in the binary GSAs by alternately varying the chemical potentials of individual graphene sheets. The evolutions of the SPP beams satisfy a negative-coupled Dirac equation in the binary GSAs, thus the beam center of SPPs undergoes a tremble motion with negative transverse shift. FDFD numerical simulations verified the plasmonic ZB as periodic spatial oscillatory motions of the SPP beams around their mean trajectories. The oscillating periods of the plasmonic ZB are strongly dependent on the propagation constant mismatch. The period of ZB varied in the range of micrometer, while the amplitude reaches tens of nanometers, which could help realizing an experimental observation of ZB. The study paves the way for using GSAs as an advantageous platform for the simulation of quantum theory in two-dimensional systems. By arranging graphene sheet waveguide in a slightly different layout, one could investigate the optical analogue of relativistic Klein tunneling at the nanoscale, as proposed and demonstrated in dielectric waveguide lattices [27,28].

973 Program (2014CB921301); National Natural Science Foundation of China (NSFC) (11104095, 11304108); Specialized Research Fund for the Doctoral Program of Higher Education of China (20130142120091).

Numerical simulations presented in this Letter were carried out using the High Performance Computing experimental testbed in SCTS/CGCL (see http://grid.hust.edu.cn/hpcc).

REFERENCES

1. W. Zawadzki and T. M. Rusin, J. Phys. Condens. Matter **23**, 143201 (2011).
2. R. Gerritsma, G. Kirchmair, F. Zähringer, E. Solano, R. Blatt, and C. F. Roos, Nature **463**, 68 (2010).
3. X. Zhang, Phys. Rev. Lett. **100**, 113903 (2008).
4. L. G. Wang, Z. G. Wang, and S. Y. Zhu, Euro. Phys. Lett. **86**, 47008 (2009).
5. S. Longhi, Opt. Lett. **35**, 235 (2010).
6. S. Ding and G. P. Wang, J. Opt. Soc. Am. B **31**, 603 (2014).
7. F. J. García de Abajo, ACS Photon. **1**, 135 (2014).
8. A. Vakil and N. Engheta, Science **332**, 1291 (2011).
9. P. Y. Chen and A. Alù, ACS Nano **5**, 5855 (2011).
10. T. Zhang, L. Chen, and X. Li, Opt. Express **21**, 20888 (2013).
11. H. Huang, B. Wang, H. Long, K. Wang, and P. Lu, Opt. Lett. **39**, 5957 (2014).
12. Y. Fan, B. Wang, K. Wang, H. Long, and P. Lu, Opt. Lett. **39**, 3371 (2014).
13. T. M. Rusin and W. Zawadzki, Phys. Rev. B **76**, 195439 (2007).
14. T. M. Rusin and W. Zawadzki, Phys. Rev. B **78**, 125419 (2008).
15. T. M. Rusin and W. Zawadzki, Phys. Rev. B **80**, 045416 (2009).
16. G. W. Hanson, J. Appl. Phys. **104**, 084314 (2008).
17. K. I. Bolotin, K. J. Sikes, Z. Jiang, M. Klima, G. Fudenberg, J. Hone, P. Kim, and H. L. Stormer, Solid State Commun. **146**, 351 (2008).
18. C. Qin, B. Wang, H. Huang, H. Long, K. Wang, and P. Lu, Opt. Express **22**, 25324 (2014).
19. B. Wang, X. Zhang, K. P. Loh, and J. Teng, J. Appl. Phys. **115**, 213102 (2014).
20. N. Christodoulides and R. I. Joseph, Opt. Lett. **13**, 794 (1988).
21. A. A. Sukhorukov and Y. S. Kivshar, Opt. Lett. **27**, 2112 (2002).
22. F. Dreisow, M. Heinrich, R. Keil, A. Tünnermann, S. Nolte, S. Longhi, and A. Szameit, Phys. Rev. Lett. **105**, 143902 (2010).
23. W. Lin and L. Chen, J. Opt. Soc. Am. B **27**, 112 (2010).
24. B. Wang, X. Zhang, X. Yuan, and J. Teng, Appl. Phys. Lett. **100**, 131111 (2012).
25. B. Wang, X. Zhang, F. J. García-Vidal, X. Yuan, and J. Teng, Phys. Rev. Lett. **109**, 073901 (2012).
26. Y. Fan, B. Wang, H. Huang, K. Wang, H. Long, and P. Lu, Opt. Lett. **39**, 6827 (2014).
27. S. Longhi, Phys. Rev. B **81**, 075102 (2010).
28. F. Dreisow, R. Keil, A. Tünnermann, S. Nolte, S. Longhi, and A. Szameit, Europhys. Lett. **97**, 10008 (2012).